Microscopic dynamics and relaxation processes in liquid hydrogen fluoride

R. Angelini,[1] P. Giura,[1] D. Fioretto,[2] G. Monaco,[1] G. Ruocco,[3] and F. Sette[1]
[1]*European Synchrotron Radiation Facility, Boîte Postale 220, F-38043 Grenoble, Cedex, France*
[2]*Universitá di Perugia and Istituto Nazionale di Fisica della Materia, I-06123, Perugia, Italy*
[3]*Universitá di Roma "La Sapienza" and Istituto Nazionale di Fisica della Materia, I-00185, Roma, Italy*
(Received 12 March 2004; revised manuscript received 14 July 2004; published 21 December 2004)

Inelastic x-ray scattering and Brillouin light scattering measurements of the dynamic structure factor of liquid hydrogen fluoride have been performed in the temperature range $T=214-283$ K. The data, analyzed using a viscoelastic model with a two time-scale memory function, show a positive dispersion of the sound velocity $c(Q)$ between the low frequency value $c_0(Q)$ and the high frequency value $c_{\infty\alpha}(Q)$. This finding confirms the existence of a structural (α) relaxation directly related to the dynamical organization of the hydrogen bonds network of the system. The activation energy E_a of the process has been extracted by the analysis of the temperature behavior of the relaxation time $\tau_\alpha(T)$ that follows an Arrhenius law. The obtained value for E_a, when compared with that observed in another hydrogen bond liquid as water, suggests that the main parameter governing the α-relaxation process is the number of hydrogen bonds per molecule.

DOI: 10.1103/PhysRevB.70.224302 PACS number(s): 63.50.+x, 61.20.−p, 61.10.Eq, 78.70.Ck

I. INTRODUCTION

To understand how the presence of a relaxation process affects the dynamics of the density fluctuations in liquids is one of the open problems in the physics of the condensed matter. Despite the fact that a large effort has been devoted to shed light on this subject, the matter is still under debate. In this respect, among all the relaxations active in a liquid, particular attention has been paid to relaxation processes of viscous nature which strongly affect the longitudinal density modes. They include at least two distinct contributions: a structural (or α) and a microscopic (or μ) process. The α process is associated to the structural rearrangement of the particles in the liquid and its characteristic time (τ_α) is strongly temperature dependent. τ_α can vary several orders of magnitude going from the ps, in the high temperature liquid phase, to $\sim$100 s in glass-forming materials at the glass transition temperature. The μ process takes its origin from the oscillatory motion of a particle in the cage of its nearest neighbors before escaping. Its characteristic time (τ_μ) is shorter than τ_α and its "strength" is often larger than the strength of the α process. Other relaxation processes, beyond the α and the instantaneous processes, associated with the internal molecular degrees of freedom may be observed in molecular liquids.[1,2] The existence of the α and μ processes, already introduced several years ago in a molecular dynamic simulation study on a Lennard-Jones fluid,[3] has recently been proved by experiments on liquid metals.[4–8] In this respect another very important class of liquids to consider is the hydrogen bonded (HB) liquid systems. In these compounds indeed, the highly directional hydrogen bond plays a crucial role in the determination of their microscopic properties. Despite the large number of theoretical studies,[9–17] the way in which the peculiarities of the hydrogen bond networks affect the static organization and the dynamical behavior of these compounds is still a subject of discussion. Many are the parameters related to the hydrogen bond that must be considered in the description of the physical properties of these liquids, as, for example, the hydrogen bond strength, the spatial network arrangement of the hydrogen bonds, and the number of hydrogen bonds per molecule. From an experimental point of view, a study of the collective dynamics as a function of these parameters is extremely important to clarify the role played by each of them on the physical properties of HB systems. Among the HB liquids, hydrogen fluoride (HF) represents one of the most intriguing systems as demonstrated by the large amount of theoretical study on its static[9–14] and dynamic[15–17] properties. It represents, in fact, a perfect HB model system: it has a simple diatomic molecule and a very strong hydrogen bond that determines a linear chain arrangement of the HB network. Nevertheless, despite its apparent simplicity, only few experimental data are available because of the very high reactivity of the material that consequently makes its handling extremely difficult. In a previous work[18] we studied the high frequency dynamics of liquid HF by inelastic x-ray scattering (IXS) at fixed temperature demonstrating the presence of both structural and microscopic relaxation processes. In the present paper we present an extended study of HF as a function of the temperature in the liquid phase between $T_B=292$ K, the boiling point, and $T_M=193$ K, the melting point. Comparing the results obtained with two different techniques, IXS and Brillouin light scattering (BLS), we find the presence of a structural relaxation process in the entire explored temperature range. The relaxation time $\tau_\alpha(T)$, in the subpicosecond time scale, follows an Arrhenius temperature dependence with an activation energy strictly related to the number of hydrogen bonds. The paper is organized as follows: Section II is devoted to the description of the experimental aspects related to the IXS and BLS measurements of the dynamic structure factor of HF. Section III is dedicated to the data analysis, in Sec. IV the main results are discussed, and finally in Sec. V the outcomes of this study are summarized.

II. SAMPLE ENVIRONMENT AND EXPERIMENTAL SETUP

High purity (99.9%) hydrogen fluoride has been purchased by Air Products and distilled in the scattering cell without further purification. The sample cell was made out of a stainless steel block, this material is well suited to resist the chemical reactivity of HF. To allow the passage of the incident and scattered beam, two sapphire windows of 250 μm thickness and 6 mm diameter have been glued on two holder plates which have then been screwed to the body of the cell. An O-ring of parofluor has been applied between the window holders and the cell to guarantee a good tightness. The whole cell has been thermoregulated by means of a liquid flux cryostat DC50-K75 Haake. Further details of the sample cell will be described elsewhere.[19]

A. Brillouin light scattering experiment

The dynamic structure factor of HF in the GHz range has been measured by Brillouin light scattering using a Sandercock-type multipass tandem Fabry-Perot interferometer characterized by high contrast ($>5\times10^{10}$), resolution [full width at half maximum (FWHM) $\approx$0.1 GHz], and a finesse of about 100. The wavelength of the incident radiation was $\lambda=514.5$ nm and the light scattered by the sample was collected in the backscattering geometry ($\theta=180°$). The free spectral range (FSR) was set to 10 GHz, the integration time was approximately 2.5 s/channel. The polarization of the incident light was vertical while the light scattered by the sample was collected in the unpolarized configuration. The aim of the present measurement is to determine the frequency position and width of the Brillouin doublets associated to the propagation of the sound modes. As the relaxation time for HF, in the investigated temperature range, is in the subpicosecond region, we do not expect any evidence of the mentioned relaxation processes in the GHz range. Thus from the measured Brillouin peak position and width, it is possible to extract information about the adiabatic sound velocity c_0 and the kinematic longitudinal viscosity ν_L.

B. Inelastic x-rays scattering experiment

The inelastic x-rays experiment has been carried out at the very high energy resolution IXS beam-line ID16 at the European Synchrotron Radiation Facility. The instrument consists of a backscattering monochromator and five independent analyzers operating at the (11 11 11) Si Bragg reflection. They are held one next to the other with a constant angular offset on a 6.5 m long analyzer arm. The used configuration[20] gives an instrumental energy resolution of 1.6 meV full width at half maximum (FWHM) and a Q offset of 3 nm^{-1} between two neighbor analyzers. The momentum transfer, Q, is selected by rotating the analyzer arm. The spectra at constant Q and as a function of energy were measured with a Q resolution of 0.4 nm^{-1} FWHM. The energy scans were performed varying the backscattering monochromator temperature with respect to that of the analyzer crystals. Further details on the beam-line are reported elsewhere.[21] Each scan took about 180 min and each spectrum at fixed Q was obtained by summing up to 3 or 6 scans.

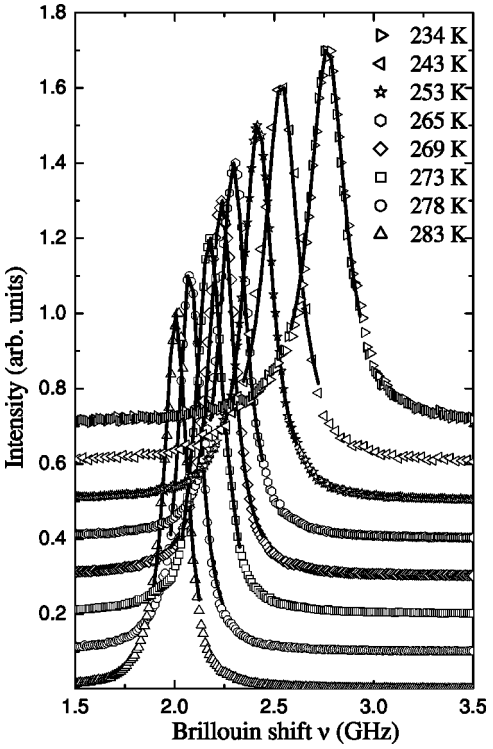

FIG. 1. Stokes part of the Brillouin light scattering spectra of HF at the indicated temperatures. The fit (solid line) are superimposed to the data (open symbols). The curves are shifted on the y axis one respect to the other.

III. DATA REDUCTION

A. Brillouin light scattering

The unpolarized Brillouin spectra were collected in a temperature range between 234 and 283 K. The quantities of interest are the position and the width of the Brillouin peaks directly related to the sound velocity c_0 and to the kinematic longitudinal viscosity ν_L of HF. In order to extract these two parameters the experimental data have been fitted in a limited region around the inelastic peaks with the function obtained by the convolution of the instrumental resolution $R(\omega)$ with a damped harmonic oscillator (DHO) function:

$$I(Q,\omega) = R(\omega) \otimes A\frac{2\Gamma(Q)\Omega(Q)^2}{[\Omega(Q)^2-\omega^2]^2+[2\omega\Gamma(Q)]^2}, \quad (1)$$

where $\Omega=2\pi\nu_0$ is the bare oscillation frequency and $2\Gamma(Q)$ is approximately the full width at half maximum (FWHM) of the sound excitations. The results of the fitting procedure are reported in Fig. 1 superimposed to the experimental data for the Stokes part of the spectra. By exploiting the relations $\Omega(Q)=c_0Q$ and $\nu_L(Q)=2\Gamma(Q)/2\pi$, the adiabatic sound velocity c_0 and the kinematic longitudinal viscosity ν_L are obtained. The exchanged momentum Q values are determined via the relation $Q=4\pi n/\lambda \sin(\theta/2)$, where n is the refractive index and θ is 180° in the used scattering geometry. The

TABLE I. Values of the frequency position ν_0 and of the width $2\Gamma(Q)$ of the Brillouin doublet as obtained by the fitting procedure described in the text. The Q values are also reported together with the sound velocities c_0 and the kinematic longitudinal viscosities ν_L.

T (K)	ν_0 (GHz)	$2\Gamma(Q)/2\pi$ (GHz)	Q (nm^{-1})	c_0 (m/s)	ν_L (cm^2/s)
234	2.74	0.24	0.029	600	0.0058
243	2.51	0.20	0.029	550	0.0049
253	2.39	0.14	0.029	530	0.0034
265	2.27	0.10	0.029	500	0.0026
269	2.21	0.09	0.028	490	0.0023
273	2.15	0.07	0.028	480	0.0017
278	2.05	0.05	0.028	450	0.0011
283	1.97	0.06	0.028	440	0.0014

temperature dependent refractive index, $n(T)$, has been obtained by using the Clausius-Mossotti relation:[22]

$$\frac{n(T)^2-1}{n(T)^2+2}=\frac{4}{3}\pi\rho_n(T)\alpha, \tag{2}$$

where ρ_n is the number density and α the optical polarizability of the HF molecule. The latter quantity, α, has been obtained using the values of $n(T\approx 293\ \mathrm{K})$ (Ref. 23) and $\rho(T\approx 293\ \mathrm{K})$ (Ref. 24) and assuming no temperature dependence for this parameter which turns out to be $\alpha=(9.606\pm0.008)\ \text{Å}^3$. The data for $n(T)$ have then been obtained at each temperature by using α and $\rho(T)$ whose expression is given by[24]

$$\rho(T)=\rho_0+A\cdot T, \tag{3}$$

with $\rho_0=(1.616\pm0.003)\ \mathrm{g/cm^3}$ and $A=-(2.25\pm0.01)\times10^{-3}\ \mathrm{g/cm^3\,K}$. The derived values of the sound velocity c_0 and the kinematic longitudinal viscosity ν_L are reported in Table I and shown in Fig. 2. It is worth noting that the error bars in Fig. 2(a) have been determined from the propagation of errors applied to the relation $c_0=2\pi\nu_0/Q$; while ν_0 is affected by statistical error coming from the fit, for Q we adopted an uncertainty arising from the maximum Q spread equivalent to $\pm3\sigma$, this gives rise to the apparently large error bars reported. The quantity $c_0(T)$ follows a linear behavior characterized by a temperature dependence well represented by the equation

$$c_0(T)=c_0+B\cdot T, \tag{4}$$

with $c_0=(1290\pm40)\ \mathrm{m/s}$ and $B=(-3.0\pm0.1)\ \mathrm{m/s\,K}$. The same procedure has been applied to derive the kinematic longitudinal viscosity ν_L for which the linear fit provides a temperature behavior described by the relation[25]

$$\ln\nu_L(T)=C+\frac{D}{T} \tag{5}$$

with $C=(-13.5\pm0.7)\ \mathrm{cm^2/s}$ and $D=(1960\pm170)\ \mathrm{cm^2\,K/s}$. All the values of Q, of the fit parameters and of the calculated ν_L and c_0, are reported in Table I.

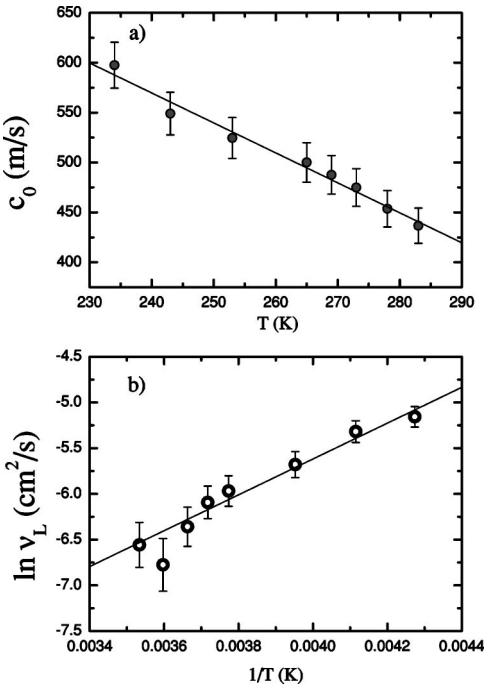

FIG. 2. (a) Sound velocity c_0 and (b) kinematic longitudinal viscosity ν_L from Table I as calculated from the position and the width of the Brillouin light scattering excitations in backscattering geometry ($\theta=180°$) (full circles). The straight lines represent the linear fit to the data.

B. Inelastic x-rays scattering

The IXS measurements, performed to probe the dynamics of HF in the mesoscopic regime, are compared to the BLS results of the previous section in order to characterize the transition from the hydrodynamic regime to the mesoscopic. In this case the $S(Q,\omega)$ has been studied at four temperatures in the range 214–283 K at $T=214$, 239, 254, and 283 K as a function of the wave vector Q. It has been varied between 1 and 15 $\mathrm{nm^{-1}}$ for all the studied temperatures except for $T=239$ K, where it has been selected between 2 and 31 $\mathrm{nm^{-1}}$. Each energy scan took 180 min and each spectrum at fixed Q was obtained by summing up to 6 or 3 scans. We report in Fig. 3 an example of the measured spectra at the investigated temperatures and at the indicated momentum transfer (symbols); they are compared with the instrumental resolution aligned and scaled to the central peak (full line). The contribution of the empty cell reported in Fig. 4 was found to be negligible compared to the total scattered intensities, however, it has been subtracted before performing the fitting procedure. The analysis of the spectra has been done within the framework of the memory function approach.[26] In this approach the classic (symmetric) $S(Q,\omega)$ is expressed as

$$S(Q,\omega)=I(Q)\frac{\omega_0(Q)^2M'(Q,\omega)}{[\omega^2-\omega_0(Q)^2-\omega M''(Q,\omega)]^2+[\omega M'(Q,\omega)]^2}, \tag{6}$$

where $\omega_0(Q)^2=[K_BT/mS(Q)]Q^2$ is the normalized second frequency moment of $S(Q,\omega)$, K_B is the Boltzmann constant, m is the mass of the molecule, and $M'(Q,\omega)$, $M''(Q,\omega)$ are,

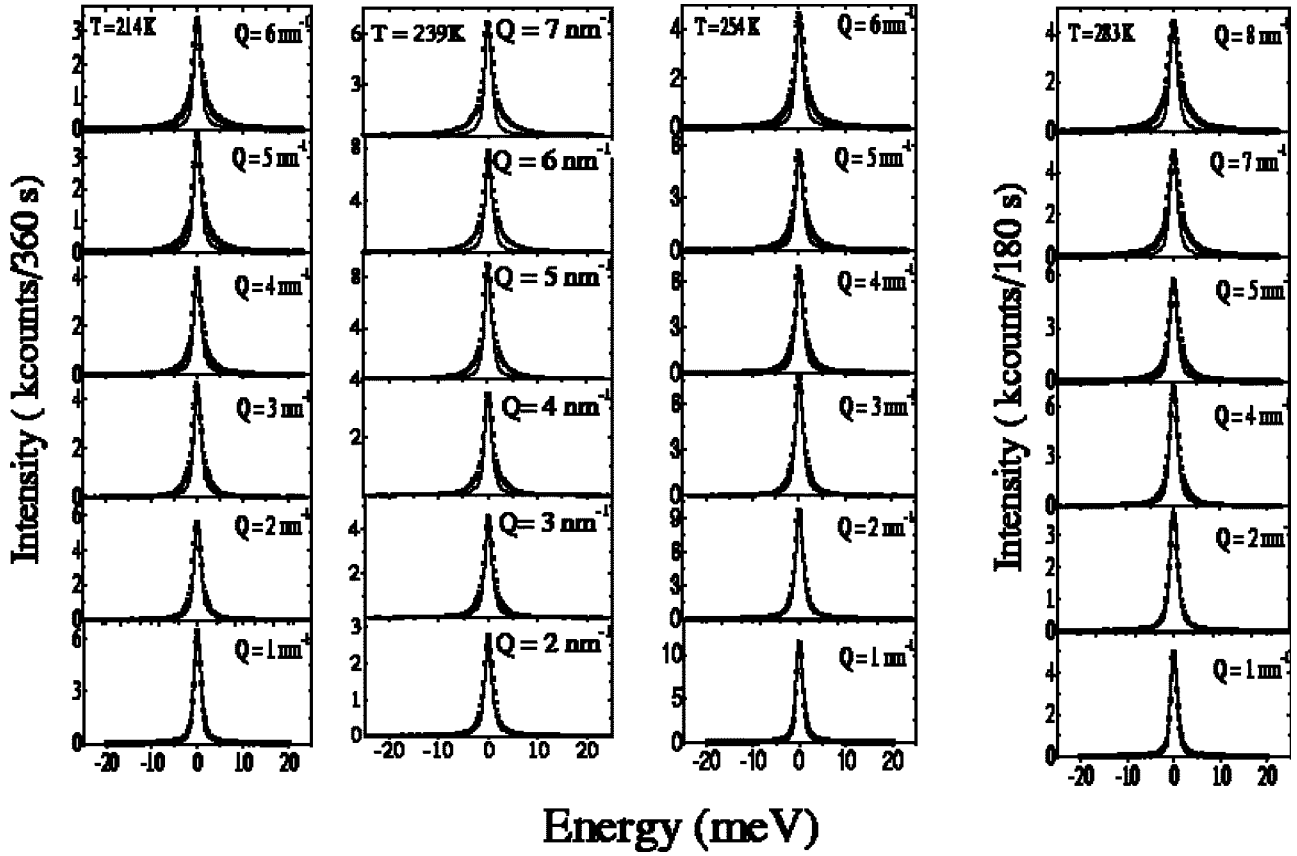

FIG. 3. IXS spectra of HF at fixed temperature in the low-Q region. The raw data (symbols) are plotted together with the corresponding experimental resolutions (full lines).

respectively, the real and the imaginary part of the Laplace transform of the memory function $M(Q,t)$. The scattered intensity is proportional to the convolution between the experimental resolution and the true ("quantum-mechanical") dynamic structure factor $S_q(Q,\omega)$:

$$S_q(Q,\omega) = \beta\hbar\omega/(1-e^{-\beta\hbar\omega})S(Q,\omega), \tag{7}$$

which is the product between the detailed balance factor and the symmetric (classical) dynamic structure factor $S(Q,\omega)$. The relation between the classic $S(Q,\omega)$ and the quantum one, $S_q(Q,\omega)$, reported in Eq. (7) is one among the different possible choices. It has been shown[27] that this specific choice correctly reproduces the (quantum) Kubo relation.

1. Markovian approach

In the Markovian approximation, the decay of the memory function is faster than any system time scale and is modeled with a δ function in the time domain[26] in such a way that Eq. (6) reduces to a DHO.

Although the correct approach to describe our data is the viscoelastic one, as we will see in the next section, a first raw analysis of the spectra has been done in terms of the Markovian approximation. In this approach one assumes that the relevant processes associated with the propagation of density fluctuations take place on a time scale much longer than the time scale $\tau(Q)$ associated with any relaxation process, i.e., $\Omega(Q)\tau(Q) \ll 1$. This means that DHO is not the more suitable

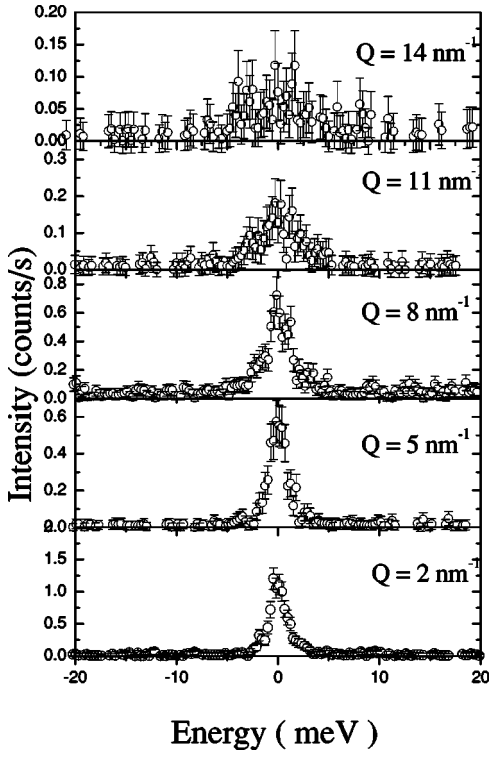

FIG. 4. A sample of the empty cell measurements at the indicated Q values for the sample cell used in the experiment.

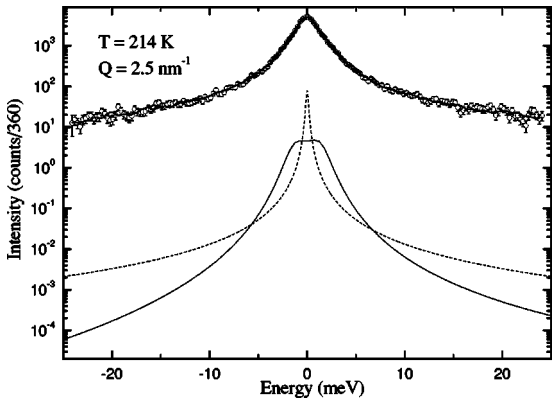

FIG. 5. An example of the measured spectrum at $T=214$ K and $Q=2.5$ nm^{-1} compared with the DHO model fit. The two resolution deconvoluted distinct quasielastic and inelastic contributions are shown scaled by a factor.

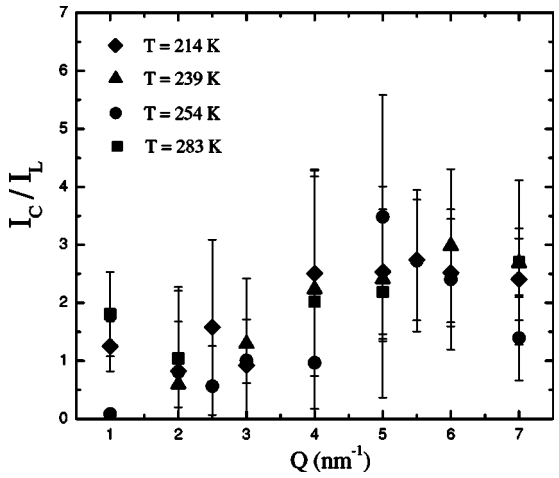

FIG. 6. Ratio between the area of the quasielastic and inelastic contributions plotted as a function of Q at the four investigated temperatures.

model to adopt in the presence of one or more relaxation processes $[\Omega(Q)\tau(Q)\sim 1]$. Nevertheless we used DHO only to make a first raw analysis of the spectra with the only aim of getting a preliminary determination of the apparent sound velocity $c(Q)=\Omega(Q)/Q$; this model in fact works well only in the limit of relaxation free response of the system. Moreover, the position of the inelastic peaks extracted through the DHO model fits well the position of the maxima of the current spectra $J(Q,\omega)=\omega^2 S(Q,\omega)$ obtained from the viscoelastic fit of the next section. The Markovian approach gives rise to a line shape in which the central line is not present, and this contribution is *a posteriori* added to the spectra through a Lorentzian line shape. Its physical origin is better understood considering the fact that, although the relaxation of thermal nature is almost absent being $\gamma=c_p/c_v$ very close to one, the presence of the Mountain peak has to be taken into account in the investigated Q region. It appears in the dynamic structure factor as a central peak of width $1/\tau_\alpha(Q)$ with $\tau_\alpha(Q)$ the structural relaxation time as better seen in the viscoelastic section. In this region in fact the condition $c(Q)Q\tau_\alpha(Q)\gtrsim 1$ is verified and the Mountain peak becomes very narrow, much narrower than the resolution function thus represented by a Lorentzian line. For this reason to fit our data we used a DHO plus a Lorentzian. In Fig. 5 we report in log-linear scale an example of the measured spectra at $T=214$ K and $Q=2.5$ nm^{-1} compared to the DHO model fit; the two distinct resolution deconvoluted quasielastic and inelastic contributions are individually shown. The ratio between the quasielastic and inelastic area of the measured spectra is reported as a function of Q and T in Fig. 6. The main parameter we are interested in is $\Omega(Q)$ which corresponds to the frequency of the sound modes. Its dispersion curve (i.e., its Q dependence) is shown in Fig. 7 at low Q for the four analyzed temperatures. The data show a common behavior in the entire investigated T range, namely a linear dependence in the Q range 4–7 nm^{-1}, with a slope corresponding to sound velocities higher than the adiabatic values c_0 measured by BLS and reported in the previous section. In addition, for lower Q, the apparent sound velocity $c(Q)$ determined by IXS seems to show a transition from the low frequency value c_0 to the higher value. This result provides the necessary information to extend what recently was observed in liquid HF at $T=239$ K (Ref. 18) to a wider temperature range. The increase of $c(Q)$ with increasing Q, in fact, is interpreted as due to the presence of a relaxation process, the structural relaxation, already observed in HF at $T=239$ K, and still present in the whole explored temperature region.

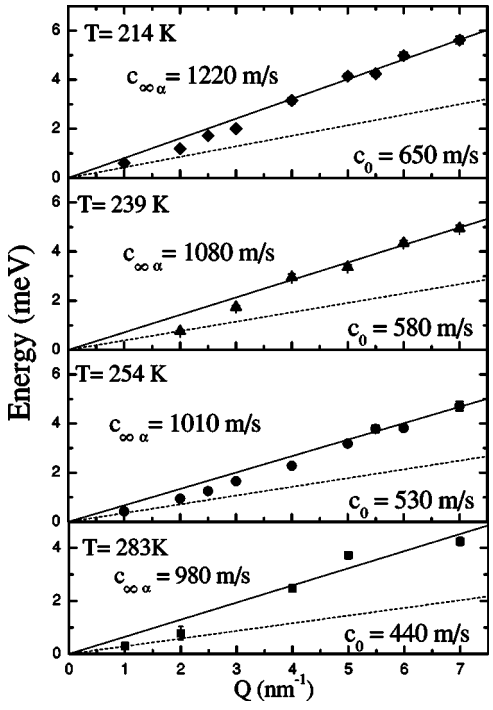

FIG. 7. Dispersion curves at the indicated temperatures. The upper full lines are the linear fits to the high-Q data. The lower dashed lines indicate the adiabatic sound velocity as measured by Brillouin light scattering as shown in Sec. II A.

2. Viscoelastic approach

The existence of a relaxation process with a characteristic time τ in the range of the probed sound waves [i.e., such that $\Omega(Q)\tau(Q) \simeq 1$], as evident from the dispersion of $\Omega(Q)$, calls for a more refined choice of the memory function with respect to the Markovian approximation. To describe the effect of this relaxation in $S(Q,\omega)$, we use the memory function based on the viscoelastic model. In this approach a two relaxation process scenario is described by a memory function $M(Q,t)$ given by the sum of two exponential decay contributions:

$$M(Q,t) = \Delta_\alpha^2(Q)e^{-t/\tau_\alpha(Q)} + \Delta_\mu^2(Q)e^{-t/\tau_\mu(Q)} \tag{8}$$

where $\Delta_\alpha^2(Q)=[c_{\infty\alpha}(Q)^2-c_0(Q)^2]Q^2$, and $\Delta_\mu^2(Q)=[c_\infty(Q)^2 - c_{\infty\alpha}(Q)^2]Q^2$ are the strengths of the two processes. As, similarly to water, one expects that the μ process is very fast with respect to the investigated time scale,[28] the second term is approximated by a δ function:

$$M(Q,t) = \Delta_\alpha^2(Q)e^{-t/\tau_\alpha(Q)} + \Gamma_\mu(Q)\delta(t) \tag{9}$$

with $\Gamma_\mu(Q)=\Delta_\mu^2\tau_\mu(Q)$. As in pure HF at $T=239$ K (Ref. 18) in fact, one expects a structural process described by an exponential decay and a microscopic process, very fast with respect to the investigate time scale[28] described by a δ function. This approach has been successfully applied in the past to describe the dynamics of simple liquids[29] and liquid metals.[5] The two contributions of Eq. (9) affect two different regions of the spectrum: the exponential decay which represents the slower relaxation process, with a relaxation time such that $\Omega(Q)\tau_\alpha(Q) \gtrsim 1$, accounts almost entirely for the quasielastic region of the spectrum (the width of the central line is of the order $1/\tau_\alpha$), its strength $\Delta_\alpha^2(Q)$ determines the apparent sound velocity through the relation $\Delta_\alpha^2(Q) =[c_{\infty\alpha}(Q)^2-c_0(Q)^2]Q^2$; the δ function which represents the faster relaxation process, such that $\Omega(Q)\tau_\mu(Q)<1$, is responsible for the width of the inelastic part. The thermal contribution in the memory function has been neglected being the value of the specific heats ratio γ close to 1. The experimental data have been fitted to the convolution of the experimental resolution function with the dynamic structure factor model given by the combination of Eqs. (6), (7), and (9). It is worth noting that, different from the Markovian approach, the viscoelastic description gives rise to a single line shape which does not allow one to separate the quasielastic and inelastic contribution. This does not make it possible to plot the analog of Figs. 5 and 6 in the case of viscoelastic analysis. The comparison of the χ^2 values obtained from the two different fitting procedures, DHO and viscoelastic, indicates the real need for the use of the latter fit function. The Q dependence of the fit parameters $c_{\infty\alpha}(Q)$, $c_0(Q)$, $\tau_\alpha(Q)$, and $\Gamma_\mu(Q)$ is described in the following.

In Fig. 8 the Q behavior of the sound velocities is shown in the low Q region and for all the investigated temperatures. Both the infinite $c_{\infty\alpha}(Q)$ and zero $c_0(Q)$ frequency limiting values, as obtained from the viscoelastic fit, are reported (open symbols). The comparison with the apparent sound velocity $c(Q)=\Omega(Q)/Q$ (closed symbols) as derived from the dispersion curve of Fig. 7, shows the transition of $c(Q)$ from $c_0(Q)$ to $c_{\infty\alpha}(Q)$. The consistency between the two independent analyses strongly suggests that this transition is governed by the α-relaxation process in the entire temperature range.

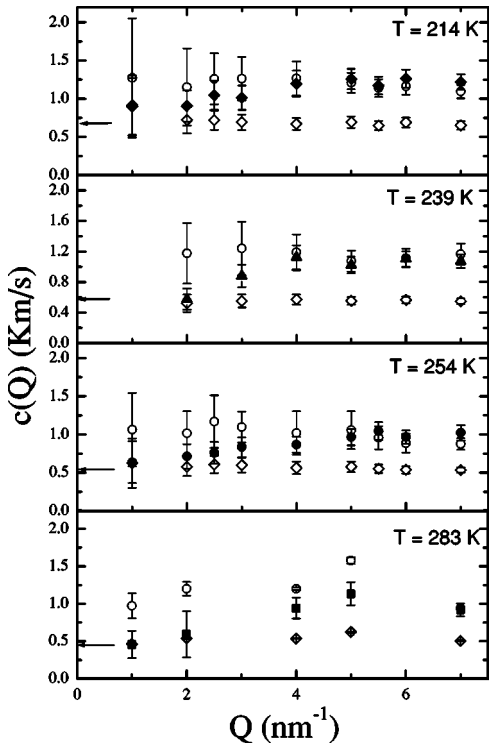

FIG. 8. Q dependence of the sound velocities $c_0(Q)$ (open diamonds) and $c_{\infty\alpha}(Q)$ (open circles) from a viscoelastic analysis, together with $c(Q)$ (closed symbols) from Fig. 7. The value of the adiabatic sound velocity, c_0, is indicated by the arrow.

The Q dependence of the relaxation time $\tau_\alpha(Q)$ is reported in Fig. 9 at the four investigated temperatures and in the Q range $1-15$ nm^{-1}. It shows a constant behavior, within the error bars, in the low Q region and a very weak decrease at increasing Q as already observed in water[28] and many other systems.[26] The fit of the data in the $1-7$ nm^{-1} range yields values $\tau_\alpha(Q\to 0)$ reported in Table II. In Fig. 10 the Q dependence of the strength of the microscopic relaxation, $\Gamma_\mu(Q)$, is reported at the four analyzed temperatures. The data show a quadratic behavior and have been fitted with a parabolic function

$$\Gamma_\mu(Q) = DQ^2.$$

The values of the parameter D are reported in Table II as a function of the temperature.

IV. DISCUSSIONS

This section is dedicated to the discussion of the temperature dependence of the low Q behavior of the different parameters analyzed in the previous paragraphs. These parameters fully characterize the collective dynamics of our system

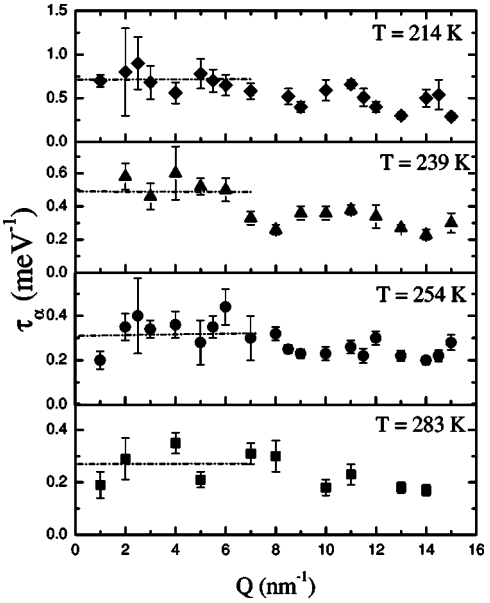

FIG. 9. Q dependence of the relaxation times $\tau_\alpha(Q)$ from the viscoelastic analysis at the indicated temperatures. A constant fit in the low Q region (dashed line) is also reported.

in the mesoscopic regime. The values of c_0, $c_{\infty\alpha}$, and $c_{\infty\alpha}/c_0$ at the four investigated temperatures are reported in Fig. 11. As shown in Fig. 11(b) the ratio $c_{\infty\alpha}/c_0$ is temperature independent in all the explored T range and it is close to two as in the case of water.[30] The temperature dependence of the structural relaxation time in the $Q\rightarrow 0$ limit has been deduced from Fig. 9. Here the low Q part of $\tau_\alpha(Q)$ has been fitted using a constant function. The obtained values are reported in Fig. 12 on a linear scale as a function of the temperature. In the explored temperature range, the $\tau_\alpha(T)$ behavior is well described by the Arrhenius law (full line):

$$\tau_\alpha(T) = \tau_0 e^{E_a/K_B T} \tag{10}$$

with an activation energy $E_a=(1.9\pm0.2)$ kcal/mol and $\tau_0=(6\pm2)10^{-15}$ s. The temperature dependence in the limit $Q\rightarrow 0$ of the last fit parameter D is reported in Table II. It yields values which appear to be temperature independent being $D=(0.170\pm0.025)$ meV/nm$^{-2}=(2.6\pm0.4)\times10^{-3}$ cm^2/s. This result is consistent with previous findings according to which the microscopic relaxation is a temperature

TABLE II. Low Q values of the parameters used to calculate the kinematic longitudinal viscosity $\nu_L(0)$ of Eq. (11): $c_0(0)$ from Eq. (4); $c_{\infty\alpha}(0)$ from the linear fit of Fig. 7; and $\tau(0)$ and Γ derived from the viscoelastic analysis as described in the text.

T (K)	$c_0(0)$ (m/s)	$c_{\infty\alpha}(0)$ (m/s)	$\tau_\alpha(0)$ (ps)	D (cm^2/s)	$\nu_L(0)$ (cm^2/s)
214	650	1220	0.47	0.0030	0.007
239	580	1080	0.32	0.0022	0.004
254	530	1010	0.21	0.0026	0.003
283	480	980	0.17	0.0026	0.003

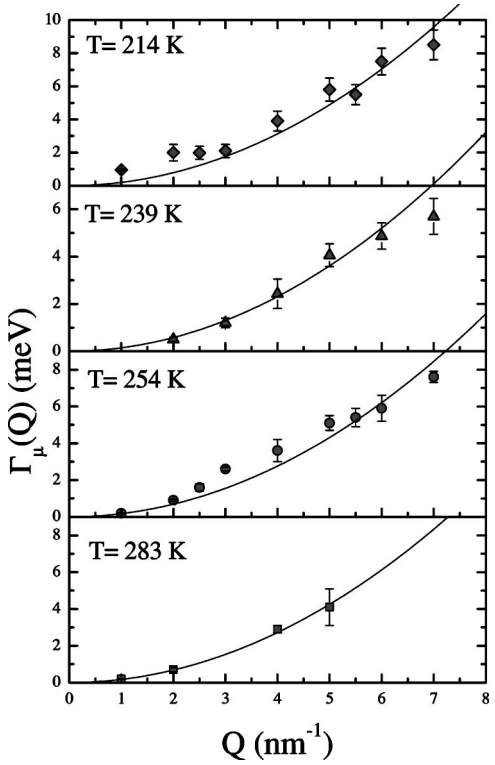

FIG. 10. Q dependence of the parameter $\Gamma_\mu(Q)$ (closed circles) in liquid HF at the analyzed temperatures from a viscoelastic analysis. The full lines are the parabolic fits to the low-Q data.

independent process.[28] Using the low Q values $\tau_\alpha(0)$ of Table II together with the low Q extrapolations of the other parameters (see Table II), it is possible to calculate the kinematic longitudinal viscosity ν_L from the relation:[26]

$$\nu_L = \tau_\alpha(0)[c^2_{\infty\alpha}(0) - c^2_0(0)] + \frac{D}{2}, \tag{11}$$

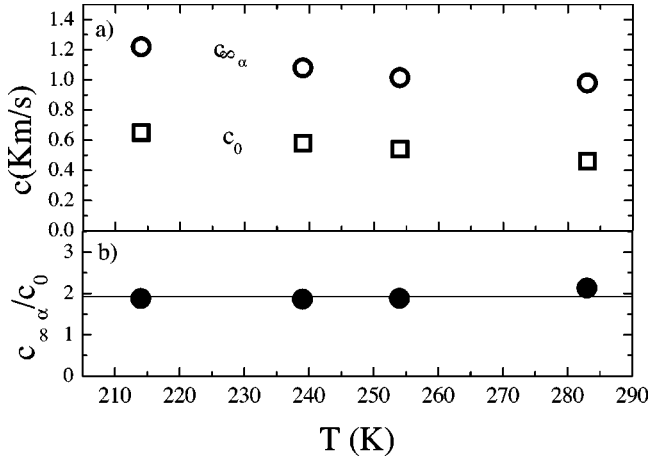

FIG. 11. (a) Behavior of the sound velocities in HF as a function of the temperature: c_0 (open squares), and $c_{\infty\alpha}$ (open circles). (b) Sound velocities ratio $c_{\infty\alpha}/c_0$ (symbols); the straight line represents a constant fit to the data.

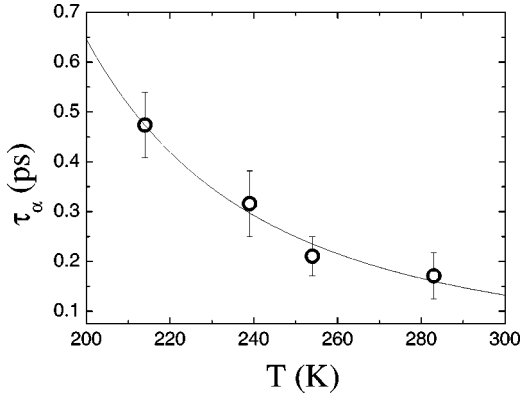

FIG. 12. T dependence of the low-Q extrapolation of the relaxation times $\tau_\alpha(Q)$ of Fig. 9 together with the Arrhenius fit (full line) of Eq. (10).

where c_0 is the adiabatic sound velocity measured by Brillouin light scattering as discussed in a previous section. The derived values for ν_L are reported in Fig. 13: they are found to be consistent with the hydrodynamic data reported in Table I. This equivalence gives further support to the validity of the employed viscoelastic model. In the same figure we also report two viscosity data determined by molecular dynamics (MD) simulations. A recent MD study of the transport coefficients (longitudinal and shear viscosity, thermal diffusivity and conductivity) of hydrogen fluoride[17] provides two values for the longitudinal viscosity η_L, one at $T=205$ K, $\eta_L(T=205\ \mathrm{K})=0.91\times10^{-2}$ g/cm s and the other at $T=279$ K, $\eta_L(T=279\ \mathrm{K})=0.38\times10^{-2}$ g/cm s. They are reported in Fig. 13 after rescaling for the density of Eq. (3) according to the relation $\nu_L(T)=\eta_L(T)/\rho(T)$, they are quite consistent with the experimental data. In Fig. 14 we report, on an Arrhenius plot, the comparison between the relaxation times for hydrogen fluoride and for water.[28] The activation energy found in water, constant in the examined temperature range, was $E_a=(3.8\pm0.6)$ kcal/mol while the one for

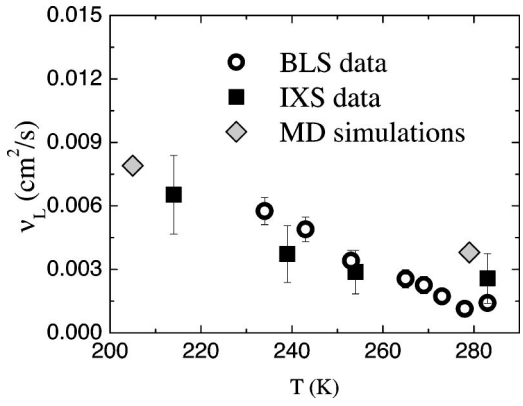

FIG. 13. Temperature dependence of the kinematic longitudinal viscosity: from IXS as calculated through Eq. (11) (closed squares), from the Brillouin light scattering values of Table I (open circles); and from molecular dynamic simulations at $T=205$ and 279 K (closed diamonds) (Ref. 17).

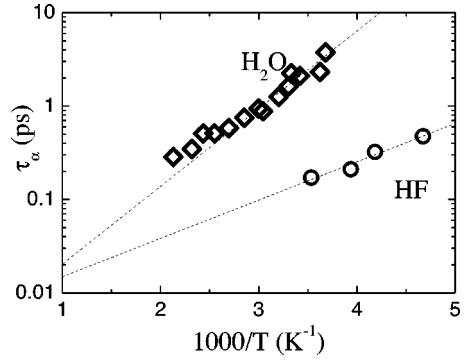

FIG. 14. Arrhenius plot for the relaxation time as obtained from viscoelastic analysis of the dynamical structure factor for water (diamonds) (Ref. 28) and hydrogen fluoride (circles). The dashed lines indicate the best linear fit to the data and their slope give an activation energy of 3.8 kcal/mol for water and 1.9 kcal/mol for HF.

hydrogen fluoride is $E_a=(1.9\pm0.2)$ kcal/mol as previously discussed. It is worthwhile to relate the values of the activation energies to the different networks present in the two liquids. While hydrogen fluoride forms linear chains with one hydrogen bond on average for each molecule, the preferred arrangement of water is the three-dimensional tetraedric structure with two hydrogen bonds for each molecule. If we indicate with $n_{\mathrm{HB-H_2O}}$ and $n_{\mathrm{HB-HF}}$ the number of hydrogen bonds for H_2O and HF, respectively, and $E_{a-\mathrm{H_2O}}$, $E_{a-\mathrm{HF}}$ the activation energies for the two liquids, we see that they satisfy the ratio

$$\frac{E_{a-\mathrm{H_2O}}}{n_{\mathrm{HB-H_2O}}} \approx \frac{E_{a-\mathrm{HF}}}{n_{\mathrm{HB-HF}}}. \tag{12}$$

In previous studies on water[31] the activation energy has been associated with that of the H-bond ($\approx$5 kcal/mol).[32] The result of Eq. (12) strengthens the idea that the structural relaxation process involves the H-bond networks of the system and it seems also to suggest that in this case the activation energy of the process is related to the number of H-bonds to make and break and not only to the strength of each H-bond.

V. CONCLUSIONS

We have presented inelastic Brillouin light and inelastic x-rays scattering measurements of liquid hydrogen fluoride, a prototype of the class of hydrogen bonded liquid systems, in a temperature range comprised between 214 and 283 K. We demonstrated that the collective dynamics of liquid HF is characterized by a structural relaxation process in the subpicosecond time scale. In the explored temperature region this relaxation process affects the collective dynamics in a Q range between 1 and 7 nm^{-1}. An accurate analysis in terms of the viscoelastic model in the memory function approach allowed one to extract and determine the temperature dependence of the parameters describing the dynamics

at microscopic level. The relaxation time related to the structural relaxation process follows an Arrhenius temperature behavior with an activation energy E_a which, compared with the value previously measured in liquid water, enables one to establish a connection between E_a and the number of hydrogen bonds per molecule of the specific system.

ACKNOWLEDGMENTS

We acknowledge R. Verbeni for assistance during the measurements, C. Henriquet for the design, development, and assembly of the hydrogen-fluoride cell, C. Lapras for technical help, and C. Alba-Simionesco, M.C. Bellissent-Funel, and J.F. Legrand for useful discussions.

[1] G. Monaco, D. Fioretto, C. Masciovecchio, G. Ruocco, and F. Sette, Phys. Rev. Lett. **82**, 1776 (1999).
[2] A. Brodin, M. Frank, S. Wiebel, G. Shen, J. Wuttke, and H. Cummins, Phys. Rev. E **65**, 051503 (2002).
[3] D. Levesque, J. Verlet, and J. Kurkijarvi, Phys. Rev. A **7**, 1690 (1973).
[4] Y. S. Badyal, U. Bafile, K. Miyazaki, I. M. de Schepper, and W. Moontfroij, Phys. Rev. E **68**, 061208 (2003).
[5] T. Scopigno, U. Balucani, G. Ruocco, and F. Sette, Phys. Rev. E **65**, 031205 (2002); **63**, 011210 (2001); Phys. Rev. Lett. **85**, 4076 (2000); J. Phys.: Condens. Matter **12**, 8009 (2000).
[6] L. E. Bove, F. Sacchetti, C. Petrillo, B. Dorner, F. Formisano, and F. Barocchi, Phys. Rev. Lett. **87**, 215504 (2001).
[7] H. Pang, Z. H. Jin, and K. Lu, Phys. Rev. B **67**, 094113 (2003).
[8] R. M. Yulmetiev, A. V. Mokshin, P. Hanggi, and V. Shurygin, Phys. Rev. E **64**, 057101 (2001).
[9] K. Honda, J. Chem. Phys. **117**, 3558 (2002).
[10] U. Rothlisberger and M. Parrinello, J. Chem. Phys. **106**, 4658 (1997).
[11] P. Jedlovszky and R. Vallauri, Mol. Phys. **92**, 331 (1997).
[12] P. Jedlovszky and R. Vallauri, J. Chem. Phys. **107**, 10166 (1997).
[13] P. Jedlovszky and R. Vallauri, Mol. Phys. **93**, 15 (1998).
[14] M. Kreitmeir, H. Bertagnoli, J. Mortensen, and M. Parrinello, J. Chem. Phys. **118**, 3639 (2003).
[15] D. Bertolini, G. Sutmann, A. Tani, and R. Vallauri, Phys. Rev. Lett. **81**, 2080 (1998).
[16] U. Balucani, D. Bertolini, G. Sutmann, A. Tani, and R. Vallauri, J. Chem. Phys. **111**, 4663 (1999).
[17] U. Balucani, D. Bertolini, A. Tani, and R. Vallauri, J. Chem. Phys. **112**, 9025 (2000).
[18] R. Angelini, P. Giura, G. Monaco, G. Ruocco, F. Sette, and R. Verbeni, Phys. Rev. Lett. **88**, 255503 (2002).
[19] R. Angelini, P. Giura, C. Henriquet, G. Monaco, R. Verbeni, G. Ruocco, and F. Sette, Rev. Sci. Instrum. (to be published).
[20] C. Masciovecchio, U. Bergmann, M. Krisch, G. Ruocco, F. Sette, and R. Verbeni, Nucl. Instrum. Methods Phys. Res. B **117**, 339 (1996).
[21] C. Masciovecchio, U. Bergmann, M. Krisch, G. Ruocco, F. Sette, and R. Verbeni, Nucl. Instrum. Methods Phys. Res. B **111**, 181 (1996).
[22] N. W. Ashcroft and N. D. Mermin, *Solid State Physics* (Harcourt College Publisher, New York, 1976).
[23] D. R. Lide, *Handbook of Chemistry and Physics-79th edition* (CCR Press, Boca Raton Fla., 1998).
[24] Landolt-Boernestein, *Numerical Data and Functional Relationships in Science and Technology* (Springer Verlag, Berlin, 1998).
[25] P. A. Egelstaff, *An Introduction to the Liquid State* (Clarendon Press, Oxford, 1992).
[26] U. Balucani and M. Zoppi, *Dynamics of the Liquid State* (Clarendon Press, Oxford, 1994).
[27] S. W. Lovesey, *Theory of Neutron Scattering From Condensed Matter* (Clarendon Press, Oxford, 1994).
[28] G. Monaco, A. Cunsolo, G. Ruocco, and F. Sette, Phys. Rev. E **60**, 5505 (1999).
[29] A. Cunsolo, G. Pratesi, R. Verbeni, D. Colognesi, C. Masciovecchio, G. Monaco, G. Ruocco, and F. Sette, J. Chem. Phys. **114**, 2259 (2001).
[30] F. Sette, G. Ruocco, M. Krisch, C. Masciovecchio, R. Verbeni, and U. Bergmann, Phys. Rev. Lett. **77**, 83 (1996).
[31] C. J. Montrose, J. A. Bucaro, J. Marshall-Croakley, and T. A. Litovitz, J. Chem. Phys. **60**, 5025 (1974).
[32] L. Pauling, *The Nature of the Chemical Bond* (Cornell University Press, Ithaca, 1939).